Applied Catalysis A: General 487 (2014) 172–180

Contents lists available at ScienceDirect

Applied Catalysis A: General

journal homepage: www.elsevier.com/locate/apcata

The application of spontaneous flocculation for the preparation of lanthanide-containing polyoxometalates intercalated layered double hydroxides: highly efficient heterogeneous catalysts for cyanosilylation

Yueqing Jia, Shen Zhao, Yu-Fei Song*

State Key Laboratory of Chemical Resource Engineering, Beijing University of Chemical Technology, Beijing 100029, P.R. China

ARTICLE INFO

Article history:
Received 12 June 2014
Received in revised form 3 September 2014
Accepted 7 September 2014
Available online 16 September 2014

Keywords:
Polyoxometalates
Lanthanide
Layered double hydroxides
Flocculation
Cyanosilylation

ABSTRACT

The lanthanide-containing polyoxometalates (POMs) have been intercalated into layered double hydroxides (LDHs) successfully through the spontaneous flocculation method, resulting in the formation of new heterogeneous LDHs–POMs catalysts Mg_3Al–LnW_{10} (Ln = Eu, Tb and Dy). The synthetic method can prevent Mg^{2+}/Al^{3+} cations leaching out of the LDHs during intercalation and successfully control the final Mg^{2+}/Al^{3+} ratio in the corresponding Mg_3Al–LnW_{10}. Most importantly, the as-prepared Mg_3Al–LnW_{10} can be obtained without the formation of the impurity phase. The heterogeneous Mg_3Al–EuW_{10} exhibits highly efficient catalytic reactivity for cyanosilylation of various aldehydes and ketones under solvent-free conditions. The Mg_3Al–EuW_{10} can be easily recovered and reused for at least 10 times without obvious decrease of catalytic activity and the composition and the structure of the Mg_3Al–EuW_{10} catalyst remain stable. Moreover, the Mg_3Al–EuW_{10}-catalyzed cyanosilylation of benzaldehyde and hexanal gives the highest TON of 119,950 and 119,906, respectively.

© 2014 Elsevier B.V. All rights reserved.

1. Introduction

Polyoxometalates (POMs) are a large class of discrete anionic metal oxides consisting of group V and VI metals in their highest oxidation states. POMs are thermally and oxidatively stable, and their chemical properties can finely be tuned by adjusting the metal ions, the heteroatoms and the counter ions [1]. These properties endow POMs superior catalytic materials that have been widely applied in industry [2]. In the case of POMs-based heterogeneous catalysts, two strategies including solidification and immobilization have been adopted up to now [3]. One of the efficient ways is the intercalation of POMs into layered double hydroxides (LDHs) to develop the heterogenized LDHs–POMs catalysts [4].

Layered double hydroxides (LDHs) are a class of layered materials with positively charged layers and the balancing anions located in the interlayer region. The general molecular formula of LDHs is $[M^{2+}_{1-x}M^{3+}_x(OH)_2](A^{n-})_{x/n}\cdot mH_2O$, where M^{2+} and M^{3+} are di- and trivalent metal cations and A^{n-} is a counteranion, $x = 0.17$–0.33 and it is defined as the $M^{3+}/(M^{2+}+M^{3+})$ ratio [5a,5b]. The interlayer anions are linked with positively charged host layer by means of electrostatic force and hydrogen bonding interactions through the water molecule of the interlayer or the hydroxyl group on the layers [5c,5d]. LDHs can provide flexible confining space that can be adjusted by changing the size and the arrangement of guest molecules. The flexible interlayer space can not only fit small-sized moieties, but also accommodate bulky catalytic sites that are difficult or even impossible to enter the rigid pores with fixed dimension [5e,5f]. Therefore, LDHs are ideal support for bulky POMs catalysts.

Generally, the LDHs–POMs catalysts can be prepared using the traditional co-precipitation, ion-exchange, and two-step ion-exchange method [6]. However, these methods show the following disadvantages that largely restrict their further application: (1) the M^{2+} and/or M^{3+} cations can leach out of the LDHs under the neutral to slightly acidic reaction conditions; (2) some POMs are hydrolytically unstable at weakly acidic to basic pH and the intercalation reactions are often accompanied by the co-formation of an impurity phase; (3) the intercalation of POMs can block the micropores of LDHs, and thereby results in low surface areas [7]; (4) the adaptability of the above-mentioned methods is in general quite poor; (5) most importantly, XRD patterns of the as-synthesized LDHs–POMs materials contain the impurity phase, which can be observed after (003) diffraction in most cases. As such, it is significant to develop new methods for the preparation of POMs intercalated LDHs.

* Corresponding author. Tel.: +86 10 64431832; fax: +86 10 64431832.
E-mail addresses: songyufei@hotmail.com, songyf@mail.buct.edu.cn (Y.-F. Song).

http://dx.doi.org/10.1016/j.apcata.2014.09.005
0926-860X/© 2014 Elsevier B.V. All rights reserved.

Recently, the exfoliated LDHs have been utilized successfully for the development of advanced functional materials. For example, Kim and co-workers [8] reported the successful assembly of negative charged polymer-encapsulated quantum dots (QDs) with the exfoliated LDH nanosheets in formamide by electrostatic interactions. Hwang and co-workers [9] reported the layer-by-layer assembly of positively charged Zn–Cr–LDH 2D nanosheets and negatively charged layered metal oxide of titanate 2D nanosheets yields mesoporous nanohybrids with an excellent photocatalytic activity. It can be naturally conceived that POMs, as a class of important metal oxides, can be assembled with LDHs in a similar way as the above-mentioned examples. Inspired by these studies [8–10], we report herein a series of new heterogeneous LDHs–POMs with the molecular formula of $Mg_{0.77}Al_{0.23}(OH)_2[EuW_{10}O_{36}]_{0.026}\cdot 0.62H_2O$ (Mg_3Al–EuW_{10}), $Mg_{0.76}Al_{0.24}(OH)_2[TbW_{10}O_{36}]_{0.027}\cdot 0.64H_2O$ (Mg_3Al–TbW_{10}) and $Mg_{0.76}Al_{0.24}(OH)_2[DyW_{10}O_{36}]_{0.027}\cdot 0.70H_2O$ (Mg_3Al–DyW_{10}) through the spontaneous flocculation method. It is worthwhile noting that the flocculation process provides a new and rational way to design new materials with a precisely controlled nanostructure. Moreover, this method can prevent Mg^{2+}/Al^{3+} cations leaching out of the LDHs during the intercalation and thereby, successfully control the final Mg^{2+}/Al^{3+} ratio in the Mg_3Al–LnW_{10} (Ln = Eu, Tb and Dy). Most importantly, the Mg_3Al–LnW_{10} materials have been obtained without the co-formation of an impurity phase. Application of the heterogeneous catalyst of Mg_3Al–EuW_{10} for cyanosilylation of various aldehydes and ketones has been carried out under solvent-free conditions, and it shows excellent cyanosilylation of benzaldehyde and hexanal with the highest TON of 119,950 and 119,906, respectively.

2. Experimental

2.1. Chemical materials

Cyclohexanone (99%), cyclooctanone (99%), 2-adamantanone (98%), 2-heptanone (97%), 2-octanone (98%), 2-nonanone (98%), 2-decanone (98%), acetophenone (99%), hexanal (99%), heptanal (99%), octanal (98%), nonanal (99%), decanal (96%), all the used aldehydes and solvents were purchased from Alfa Acesa. Analytical europium (III) chloride hexahydrate ($EuCl_3\cdot 6H_2O$), terbium (III) chloride hexahydrate ($TbCl_3\cdot 6H_2O$), dysprosium (III) chloride hexahydrate ($DyCl_3\cdot 6H_2O$), acetic acid (CH_3COOH), sodium tungstate ($Na_2WO_4\cdot 2H_2O$), magnesium nitrate ($Mg(NO_3)_2\cdot 6H_2O$), aluminum nitrate ($Al(NO_3)_3\cdot 6H_2O$), hexamethylenetetramine (HMT) and nitric acid (65 wt.% HNO_3) were obtained from Energy Chemical in Shanghai. All the chemicals and solvents were used without further purification.

2.2. Measurements

Powder X-ray diffraction (XRD) patterns were recorded on a Rigaku XRD-6000 diffractometer under the following conditions: 40 kV, 30 mA, Cu Kα radiation (λ = 0.154 nm). Fourier transform infrared (FT-IR) spectra were recorded on a Bruker Vector 22 infrared spectrometer using KBr pellet method. Thermogravimetric and differential thermal analyses (TG-DTA) were performed on a TGA/DSC 1/1100 SF from Mettler Toledo in flowing N_2 with a heating rate of 10 °C min^{-1} from 25 to 1000 °C. Scanning electron microscopy (SEM) images and energy dispersive X-ray (EDX) analytical data were obtained using a Zeiss Supra 55 SEM equipped with an EDX detector. Transmission electron microscopy (TEM) micrographs were recorded using a Hitachi H-800 instrument. Inductively coupled plasma-atomic emission spectroscopy (ICP-AES) analysis was performed using a Shimadzu ICPS-7500 spectrometer. BET measurements were performed at 77 K on a QuantachromeAutosorb-1C analyzer. The samples were degassed at 110 °C for 6 h before the measurements. X-ray photoelectron spectroscopy (XPS) measurements were performed with monochromatized Al Kα exciting X-radiation (PHI Quantera SXM). The temperature-programmed desorption of ammonia and carbon dioxides (NH_3/CO_2-TPD) were obtained using Auto Chem. II 2920 equipment to examine acid and basic properties of the catalysts surface, respectively. The measurements were accomplished with 0.050 g of a sample in the temperature range from 100 to 700 °C, with helium (He) as a carrier gas and NH_3/CO_2 as adsorbing gas. Prior to the measurements, the samples were heated in the flow of He at 500 °C. After cooling the samples in He to 100 °C, the heating rate of 20 °C min^{-1} was applied. The corresponding cyanohydrins were analyzed by Agilent 7820A gas chromatography (GC) system using a 30 m 5% phenylmethyl silicone capillary column with an ID of 0.32 mm and 0.25 μm coating (HP-5). Yields were determined by GC analysis using reference standards. Assignments of corresponding cyanohydrins were analyzed by ^{1}H-NMR. ^{1}H-NMR spectra was recorded on a Bruker 400 MHz NMR spectrometer.

2.3. Preparation of the Na–LnW_{10} and Mg_3Al–NO_3

$Na_9LnW_{10}O_{36}$ (Na–LnW_{10}; Ln=Eu, Tb and Dy) [11], $[Mg_{0.75}Al_{0.25}(OH)_2](CO_3)_{0.125}\cdot 2H_2O$ (denoted as Mg_3Al–CO_3) [12], $[Mg_{0.75}Al_{0.25}(OH)_2](NO_3)_{0.25}\cdot 2H_2O$ (Mg_3Al–NO_3) [12] can be prepared according to literature methods.

2.4. Preparation of the Mg_3Al–LnW_{10}

An amount of 0.10 g of Mg_3Al–NO_3–LDHs was mixed with 100 ml of formamide in a flask, which was tightly sealed after purging with N_2 to avoid carbonate contamination. The mixture was vigorously stirring for 2 days. The nanosheet suspension was obtained after separating an un-exfoliated component by centrifugation for 10 min [13].

Na–LnW_{10} (0.35 g, 0.11 mmol) was dissolved in 10 ml H_2O (Ln = Eu, Tb and Dy). The Mg_3Al–LnW_{10} was synthesized by mixing the nanosheets suspension of Mg_3Al–NO_3 and the solution of Na–LnW_{10} with stirring under N_2 atmosphere for 1 day. The restacked Mg_3Al–LnW_{10} was obtained by centrifugation, washed with ethanol and water thoroughly, and then dried under vacuum.

For Mg_3Al–EuW_{10}, 0.11 g (yield = 89%); XRD (Cu Kα,): 2θ = 6.958 (003), 16.046 (006), 28.665 (012), 36.553 (015), 61.279 (110). FT-IR (KBr, cm^{-1}): ν = 3423, 947, 884, 699, 447. XPS (eV): 35.6 ($W4f_{7/2}$), 37.7 ($W4f_{5/2}$), 74.7 (Al_{2p}), 1134.3 (Eu_{3d5}), 1303.7 (Mg_{1s}). Elemental analysis (%)—found: Mg 13.81, Al 4.39, W 35.01, Eu 2.93; Cacld. For $Mg_{0.77}Al_{0.23}(OH)_2[EuW_{10}O_{36}]_{0.026}\cdot 0.62H_2O$: Mg 13.68, Al 4.54, W 34.93, Eu 2.89. For Mg_3Al–TbW_{10}, 0.11 g (yield = 88%); XRD (Cu Kα,°): 2θ = 7.082 (003), 16.012 (006), 28.724 (012), 36.777 (015), 61.329 (110). FT-IR (KBr, cm^{-1}): ν = 3442, 949, 882, 699, 448. XPS (eV): 35.6 ($W4f_{7/2}$), 37.7 ($W4f_{5/2}$), 74.6 (Al_{2p}), 1244.4 (Tb_{3d5}), 1303.6 (Mg_{1s}). Elemental analysis (%)—found: Mg 13.27, Al 4.49, W 35.52, Tb 3.11; Cacld. For $Mg_{0.76}Al_{0.24}(OH)_2[TbW_{10}O_{36}]_{0.027}\cdot 0.64H_2O$: Mg 13.20, Al 4.63, W 35.46, Tb 3.07. For Mg_3Al–DyW_{10}, 0.10 g (yield = 82%); XRD (Cu Kα,°): 2θ = 7.082 (003), 16.090 (006), 28.411 (012), 36.465 (015), 61.172 (110). FT-IR (KBr, cm^{-1}): ν = 3424, 947, 880, 698, 447. XPS (eV): 35.6 ($W4f_{7/2}$), 37.7 ($W4f_{5/2}$), 74.6 (Al_{2p}), 1295.0 (Dy_{3d5}), 1303.6 (Mg_{1s}). Elemental analysis for $Mg_{0.76}Al_{0.24}(OH)_2$ $[DyW_{10}O_{36}]_{0.027}\cdot 0.70H_2O$ (%)—found: Mg 13.15, Al 4.52, W 35.21, Dy 3.13; Cacld: Mg 13.09, Al 4.59, W 35.17, Dy 3.11.

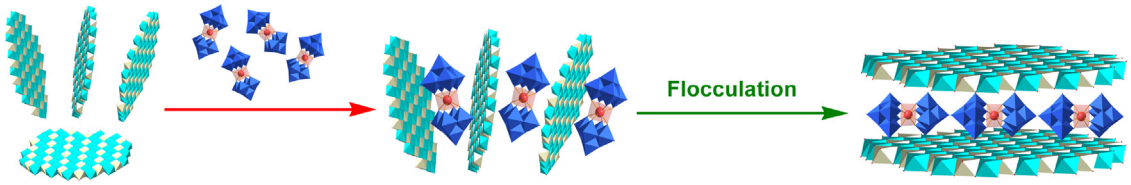

Scheme 1. The preparation process of Mg_3Al–LnW_{10} using the spontaneous flocculation method.

2.5. Procedure for cyanosilylation

In a typical experiment, 1 mmol aldehyde or ketone, 1.5 mmol TMSCN and Mg_3Al–LnW_{10} (0.25 mol% LnW_{10} to substrate, Ln = Eu, Tb and Dy) as catalyst were placed in a 20 ml glass bottle at 25 °C and the reaction mixture was kept stirring vigorously. The yield of cyanohydrin was periodically determined by GC analysis by reference standards. After the reaction was completed, the resulting oily product was extracted by diethyl ether. The catalyst of Mg_3Al–LnW_{10} was recovered by centrifugation, washed with acetone, and dried in air. The corresponding cyanohydrin was obtained by column chromatography on silica gel, and the isolated yield could be calculated based on the obtained cyanohydrin.

3. Results and discussion

3.1. Preparation of the Mg_3Al–LnW_{10}

Scheme 1 shows the process of the preparation of Mg_3Al–LnW_{10} using the spontaneous flocculation method. First of all, the precursor of $[Mg_{0.75}Al_{0.25}(OH)_2](NO_3)_{0.250}{\cdot}2H_2O$ (Mg_3Al–NO_3) can be prepared from $[Mg_{0.75}Al_{0.25}(OH)_2](CO_3)_{0.125}{\cdot}2H_2O$ (Mg_3Al–CO_3) through acid–alcohol mixed method [14]. The positive nanosheets of $[Mg_{0.75}Al_{0.25}(OH)_2]^{0.25+}$ can be obtained by exfoliation of Mg_3Al–NO_3 in formamide. The positive Mg_3Al–NO_3 nanosheets can be confirmed to be unilamellar with lateral dimensions of 2–3 μm, which are consistent with previous studies [15]. Secondly, the aqueous solution of POMs is added to the positive Mg_3Al–NO_3 nanosheets suspension. They are reconstructed into the Mg_3Al–LnW_{10} nanohybrids that are precipitated from the reaction mixture. Finally, the Mg_3Al–LnW_{10} nanohybrids can be obtained by centrifugation through the spontaneous flocculation of the positive Mg_3Al–NO_3 nanosheets and the negative POMs clusters. Furthermore, the acid resistance of LDHs is much higher in organic solvents than that in water [14], which can reduce largely the co-formation of the impurity phase the Mg^{2+} rich salt of the POMs.

3.2. Characterization of the Mg_3Al–LnW_{10}

The powder XRD patterns of Mg_3Al–EuW_{10}, Mg_3Al–TbW_{10} and Mg_3Al–DyW_{10} (Fig. 1A) show five Bragg diffraction peaks in the range of $5° < 2\theta < 70°$. XRD patterns of Mg_3Al–EuW_{10}, Mg_3Al–TbW_{10} and Mg_3Al–DyW_{10} are fully indexed to a hexagonal unit cell belonging to the *R-3m* space group. The corresponding basal spacing of *d*(003) has been summarized in Table S1. Taking Mg_3Al–EuW_{10} as an example, the gallery height value of 0.79 nm can be obtained by subtracting the thickness of host layer (0.48 nm) from the value of *d*(003) spacing of Mg_3Al–EuW_{10}. The gallery height is nearly the same as the diameter of the short axis of EuW_{10} [11], which indicates that the intercalated EuW_{10} anions are arranged in an orientation angle of θ ($\theta = 90°$) with respect to the Mg_3Al–LDHs layers. The other Mg_3Al–LnW_{10} catalysts of Mg_3Al–TbW_{10} and Mg_3Al–DyW_{10} are in the similar case.

It is very common to observe the impurity phase neighboring (003) diffraction in the XRD patterns of LDHs–POMs by traditional synthetic methods such as ion exchange, co-precipitation, etc. [4,16] and this impurity phase is often attributed to the co-formation of the salt of the POMs [7]. Interestingly, the XRD patterns of Mg_3Al–LnW_{10} do not exhibit such impurity phase.

FT-IR spectra of Mg_3Al–EuW_{10}, Na–EuW_{10} and Mg_3Al–NO_3 are shown in Fig. 2. The sharp and narrow absorption band at 1378 cm^{-1} in the spectrum of Mg_3Al–NO_3 is due to the characteristic stretching vibration of NO_3^- groups [17]. In the case of Na–EuW_{10}, the strong absorption band at 946, 880 and 697 cm^{-1} can be assigned to the W–O_t, W–O_c–W and W–O_e–W asymmetric stretching vibrations, respectively. For the FT-IR spectrum of Mg_3Al–EuW_{10}, the broad band at ca. 3423 cm^{-1} is assigned to the O–H stretching vibration in the brucite-like layers, and it is noted that this absorption is located at much lower frequency than that of free water at 3600 cm^{-1} [18], which might result from the hydrogen bonding between interlayer water and hydroxyl groups of the host layers [19]. The characteristic absorption bands for the W–O shift from 946, 880 and 697 cm^{-1} in Na–EuW_{10} to higher frequency at 947, 884 and 699 cm^{-1} in Mg_3Al–EuW_{10}, indicating the presence of strong electrostatic interactions between the host layers and the guest anions [4]. The absorption band at 447 cm^{-1} can be ascribed

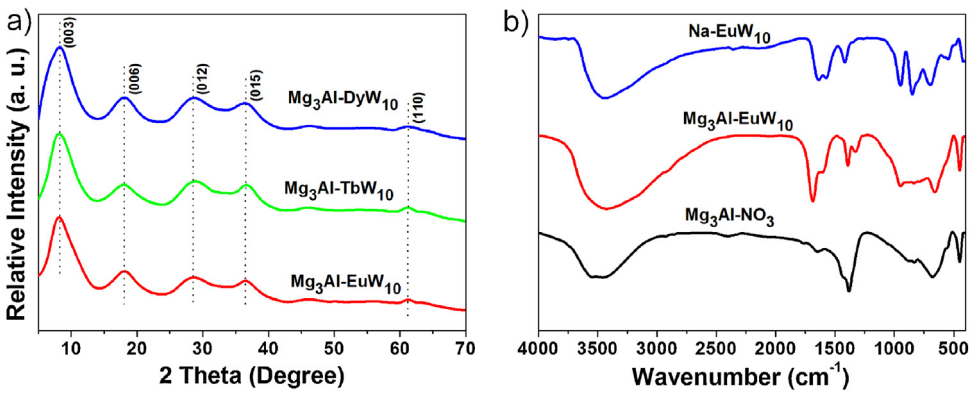

Figure 1. (A) Powder XRD patterns of Mg_3Al–EuW_{10}, Mg_3Al–TbW_{10} and Mg_3Al–DyW_{10}; (B) FT-IR spectra of Mg_3Al–NO_3, Mg_3Al–EuW_{10} and Na–EuW_{10}.

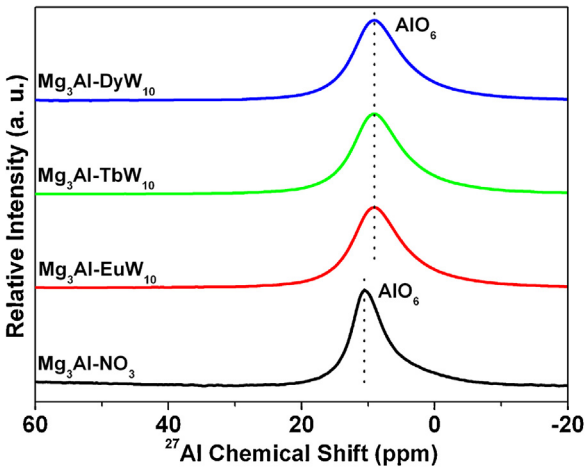

Figure 2. The ^{27}Al-MAS-NMR spectra of Mg_3Al–NO_3, Mg_3Al–EuW_{10}, Mg_3Al–TbW_{10} and Mg_3Al–DyW_{10}.

to O–M–O (M = Mg and Al) vibrations in the brucite-like layers of the LDH [20]. Compared with that of Mg_3Al–NO_3, the disappearance of the absorption band at 1378 cm^{-1} for nitrate anions and the presence of the stretching bands of EuW_{10} in the FT-IR spectrum of Mg_3Al–NO_3 indicates the successful formation of the LDHs–POMs. FT-IR spectra of Mg_3Al–TbW_{10} and Mg_3Al–DyW_{10} can be explained in a similar way (Figs. S2 and S3).

Solid state ^{27}Al-MAS-NMR has been used to estimate the local environments of Al^{3+} in the corresponding LDHs–POMs. As is known, the ^{27}Al resonance line positions are very sensitive to the coordination number and are expected to occupy the −5 to 15 ppm range for the octahedral geometry (AlO_6) sites [21]. The ^{27}Al-MAS-NMR spectrum of Mg_3Al–NO_3 shows only one peak at 10.50 ppm (Fig. 2), indicating all the Al^{3+} in Mg_3Al–NO_3 possess the octahedral structural geometry. In the case of Mg_3Al–EuW_{10}, only one peak at 9.07 ppm is visible in the ^{27}Al-MAS-NMR spectrum, suggestiong the Al^{3+} in Mg_3Al–EuW_{10} also possess the octahedral structural geometry. The above results reveal that the structure of LDHs remains unchanged after the interacalation of EuW_{10}. The peak shift in the ^{27}Al-MAS-NMR spectra is due to the intercalation of EuW_{10} into LDHs [22]. Similar explanation can be applied to the ^{27}Al-MAS-NMR results of Mg_3Al–TbW_{10} and Mg_3Al–DyW_{10}. The assignments of ^{27}Al-MAS-NMR spectra of Mg_3Al–NO_3, Mg_3Al–EuW_{10}, Mg_3Al–TbW_{10} and Mg_3Al–DyW_{10} can be found in Table S7.

The XPS spectra corresponding to Mg core levels of the Mg_3Al–EuW_{10} and Mg_3Al–NO_3 are shown in Fig. 3A. The binding energy of Mg_{1s} is 1303.7 eV in the Mg_3Al–EuW_{10}, and that is 1303.6 eV in the Mg_3Al–NO_3. The XPS spectra corresponding to Al core levels of the Mg_3Al–EuW_{10} and Mg_3Al–NO_3 are shown in Fig. 3B. The binding energy of Al_{2p} is 74.7 eV in the Mg_3Al–EuW_{10}, and 74.6 eV in the Mg_3Al–NO_3. The binding energy of $W4f_{7/2}$ and $W4f_{5/2}$ are 35.6 and 37.7 eV in the Mg_3Al–EuW_{10}, while 35.5 and 37.6 eV in the Na–EuW_{10} (Fig. 3C). Similarly, it can be observed that the binding energy of Eu_{3d5} is 1134.3 eV in the Mg_3Al–EuW_{10}, and 1134.1 eV in the Na–EuW_{10} (Fig. 3D). The above results reveal that the binding energy of Mg_{1s} and Al_{2p} in the Mg_3Al–EuW_{10} are almost the same as those of the Mg_3Al–NO_3. The $W4f_{7/2}$ and $W4f_{5/2}$ peak width of Mg_3Al–EuW_{10} is slightly different from that of Na–EuW_{10}, and such difference is dues to the interactions between the LDHs layers and EuW_{10} in Mg_3Al–EuW_{10}. XPS results of Mg_3Al–TbW_{10} and Mg_3Al–DyW_{10} can be explained in a similar way (Figs. S4 and S5).

TG-DTA curve for Mg_3Al–EuW_{10} is shown in Fig. S6. Three weight-loss stages can be observed with the increase of the temperature from 25 to 1000 °C. The first weight loss is 7.98% between 30 and 242 °C, which is attributed to the removal of water molecules (Calcd. 0.62H_2O per Mg_3Al–EuW_{10}). The second weight loss step of 8.94% at 242–476 °C can be attributed to the collapse of the

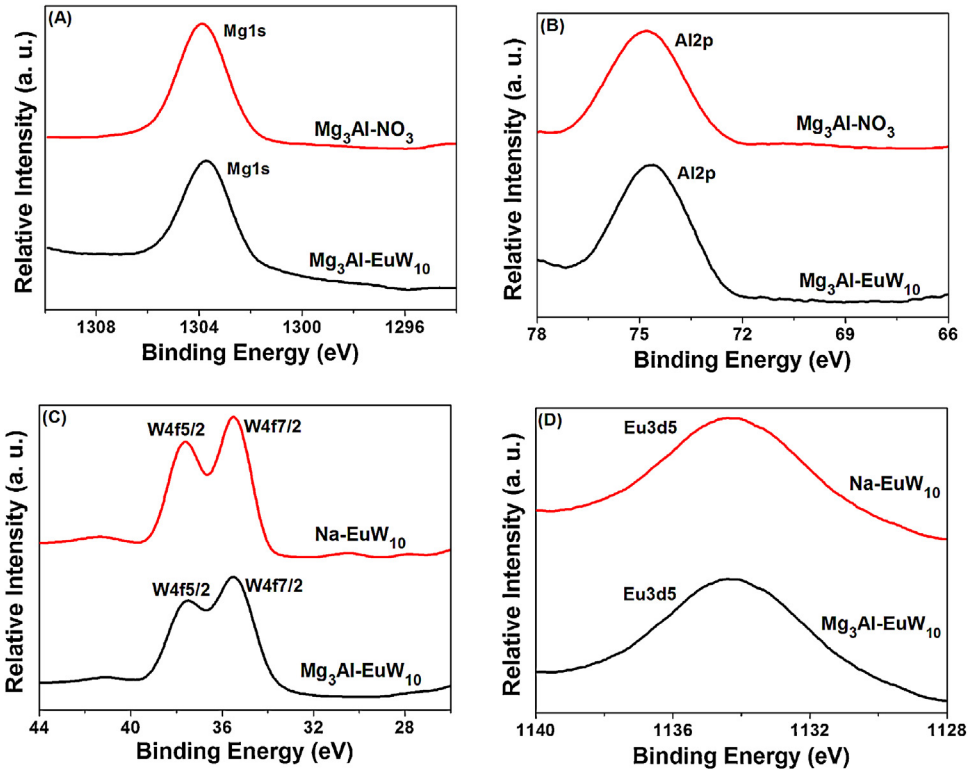

Figure 3. The XPS spectra of Mg_3Al–EuW_{10}.

Table 1
BET and TPD results of Mg_3Al–EuW_{10}, Mg_3Al–TbW_{10} and Mg_3Al–DyW_{10}.

Entry	Catalyst	Surface area ($m^2\ g^{-1}$)	Pore volume ($cm^3\ g^{-1}$)	Pore size (nm)	Total acidity (mmol NH_3 $gcat^{-1}$)[a]	Total basicity (mmol CO_2 $gcat^{-1}$)[b]
1	Mg_3Al–EuW_{10}	33	0.09	4.2	1.09	1.31
2	Reused Mg_3Al–EuW_{10}	32	0.09	4.2	1.08	1.29
3	Mg_3Al–TbW_{10}	42	0.17	3.8	1.05	1.24
4	Mg_3Al–DyW_{10}	29	0.06	4.2	1.08	1.27

[a] The amount of acid sites were calculated by quantifying the desorbed NH_3 from NH_3-TPD.
[b] The amount of basic sites were calculated by quantifying the desorbed CO_2 from CO_2-TPD.

layered structure. The third weight loss of 1.12% at 476–591 °C corresponds to partial decomposition of interlayer EuW_{10}. Similar explanation can be applied to the TG-DTA results of Mg_3Al–TbW_{10} and Mg_3Al–DyW_{10} (Figs. S7 and S8). Combining the TG-DTA and ICP analysis (Table S9), the molecular formula of Mg_3Al–LnW_{10} can be determined.

SEM and TEM images of Mg_3Al–EuW_{10}, Mg_3Al–TbW_{10} and Mg_3Al–DyW_{10} (Fig. 4) show the porous stacking of sheet-like crystallites. The particle sizes of these crystallites are 300–400 nm. Mg_3Al–EuW_{10} shows a type I adsorption isotherm at relative lower pressure ($P/P_0 < 0.1$), and a H_3 type N_2 hysteresis loop at relative higher pressure ($P/P_0 > 0.5$) according to BDDT (Brunauer, Deming, Deming and Teller) classification (Fig. S9) [23], indicating the presence of both interlayer micropores and inter-particle mesopores. Mg_3Al–TbW_{10} and Mg_3Al–DyW_{10} exhibit similar situation (Figs. S10 and S11). Temperature-programmed desorption of ammonia (NH_3-TPD) demonstrate that the Mg_3Al–EuW_{10} exhibit a main NH_3 desorption peak at 378.4 °C in Fig. 5A, which corresponds to the NH_3 molecules adsorbed on medium acid sites (both Brónsted and Lewis acid sites) of lanthanide-containing POMs of EuW_{10}. Temperature-programmed desorption of carbon dioxide (CO_2-TPD) demonstrate that the Mg_3Al–EuW_{10} exhibit a main CO_2 desorption peak at 369.3 °C in Fig. 5B, which corresponds to the CO_2 molecules adsorbed on medium basic sites of Mg_3Al–LDHs. The total acidity and basicity of the Mg_3Al–EuW_{10}, Mg_3Al–TbW_{10} and Mg_3Al–DyW_{10} determined by NH_3-TPD and CO_2-TPD have been summarized in Table 1. The results reveal that the Mg_3Al–LnW_{10} catalysts can provide both acidity and basicity.

3.3. Catalytic performance of the Mg_3Al–LnW_{10}

The cyanosilylation of aldehydes and ketones with trialkylsilyl cyanides (TMSCNs) is of significance in organic synthesis because this reaction not only creates a new C–C bond, but also protects an alcohol function. Cyanohydrins produced by this method can be transformed into a variety of building blocks, such as α-hydroxy acids, α-hydroxy ketones and β-amino alcohols [24], which are widely applied in chemical industry. Among the catalysts developed for the cyanosilylation reaction, both acid catalysts [25] and base catalysts [26] can act as catalysts to promote cyanosilylation. Therefore, from molecular structural viewpoint, design of acid–base catalysts is a promising pathway to develop efficient catalysts for such cyanosilylation reaction. As such, the Mg_3Al–LnW_{10} catalysts with both acidity and basicity have been applied for cyanosilylation of various aldehydes and ketones under solvent-free conditions.

Cyanosilylation of acetophenone catalyzed by Mg_3Al–EuW_{10} has been carried out at 25 °C under solvent-free conditions, and excellent yield of 95% with >99.9% selectivity of corresponding cyanohydrin can be obtained (Table 2, Entry 1). Other LDHs–POMs of Mg_3Al–TbW_{10} and Mg_3Al–DyW_{10} only give the yields of 72 and 48% (Entries 2 and 3), which are much lower than that of Mg_3Al–EuW_{10}. The lanthanide-containing POMs of $Na_9[EuW_{10}O_{36}]$, $K_{11}[Eu(PW_{11}O_{39})_2]$, $K_{13}[Eu(SiW_{11}O_{39})_2]$ and $K_{17}[Eu(P_2W_{17}O_{61})_2]$ (Na–EuW_{10}, K–$Eu(PW_{11})_2$, K–$Eu(SiW_{11})_2$ and K–$Eu(P_2W_{17})_2$) are not effective (Entries 4–7). The Keggin-type POMs of $H_3[PW_{12}O_{40}]$, $Na_3[PW_{12}O_{40}]$, $H_4[SiW_{12}O_{40}]$ (H–PW_{12}, Na–PW_{12} and H–SiW_{12}; Entries 8–10), and the lacunary Keggin-type POMs of $K_7[PW_{11}O_{39}]$, $Na_8H[A\text{-}PW_9O_{34}]$, $Na_8H[B\text{-}PW_9O_{34}]$, $K_8[SiW_{11}O_{39}]$ and $Na_{10}[SiW_9O_{34}]$ (K–PW_{11}, Na–A–PW_9, Na–B–PW_9, K–SiW_{11} and Na–SiW_9, Entries 11–15) show almost no catalytic efficiency.

Table 2
The effect of different catalysts on cyanosilylation of acetophenone with TMSCN at 25 °C under solvent-free condition.

Entry	Catalyst	Yield (%)
1	Mg_3Al–EuW_{10}	95
2	Mg_3Al–TbW_{10}	72
3	Mg_3Al–DyW_{10}	48
4	Na–EuW_{10}	7
5	K–$Eu(PW_{11})_2$	7
6	K–$Eu(SiW_{11})_2$	6
7	K–$Eu(P_2W_{17})_2$	6
8	H–PW_{12}	5
9	Na–PW_{12}	5
10	H–SiW_{12}	4
11	K–PW_{11}	7
12	Na–A–PW_9	8
13	Na–B–PW_9	9
14	K–SiW_{11}	5
15	Na–SiW_9	6
16	Mg_3Al–NO_3	7
17	Mg_3Al–NO_3 + Na–EuW_{10}	33
18	Na_2WO_4	8
19	$EuCl_3$	48
20	$EuCl_3$ + Na_2WO_4	49
21	None	7

Reaction conditions: acetophenone (1 mmol), catalyst (2.5 mol% W to acetophenone), 25 °C, 6 h. Yields were determined by GC analysis using reference standards. Assignments of corresponding cyanohydrins were analyzed by ^{1}H- and ^{13}C-NMR.

Contrast experiments suggest that the LDHs precursor of Mg_3Al–NO_3 is not effective (Entry 16). The physical mixture of Mg_3Al–NO_3 and Na–EuW_{10} gives the yield of 33%, which is much lower than that of Mg_3Al–EuW_{10} (Entry 17). Na_2WO_4 is not effective (Entry 18). $EuCl_3$ and the physical mixture of $EuCl_3$ and Na_2WO_4 give the yields of 48 and 49%, respectively (Entries 19 and 20). These yields are much lower than that of Mg_3Al–EuW_{10}. The reaction cannot proceed in the absence of catalyst (Entry 21). The above results reveal that Mg_3Al–EuW_{10} gives the best catalytic activity, and the catalytic activity decreases with the decrease of the ionic radii of Ln^{3+} in Mg_3Al–LnW_{10} (Eu^{3+} (1.21 Å) > Tb^{3+} (1.18 Å) > Dy^{3+} (1.17 Å) for eight coordination). The above results reveal that interactions between the Ln^{3+} cations and the two sandwiching $[W_5O_{18}]^{6-}$ POM units weaken with an increase of ionic radii of the Ln^{3+} cations, which suggests that the steric crowding around the Ln^{3+} centers decreases with an increase in ionic radii of Ln^{3+} cations [29]. During the reaction, the weaker interaction between the Ln^{3+} cations and the two sandwiching $[W_5O_{18}]^{6-}$ POM units results in the stronger interaction between the Ln^{3+} cations and carbonyl groups. Therefore, the carbonyl groups can be better activated by the Ln^{3+} cations with larger radii, and the

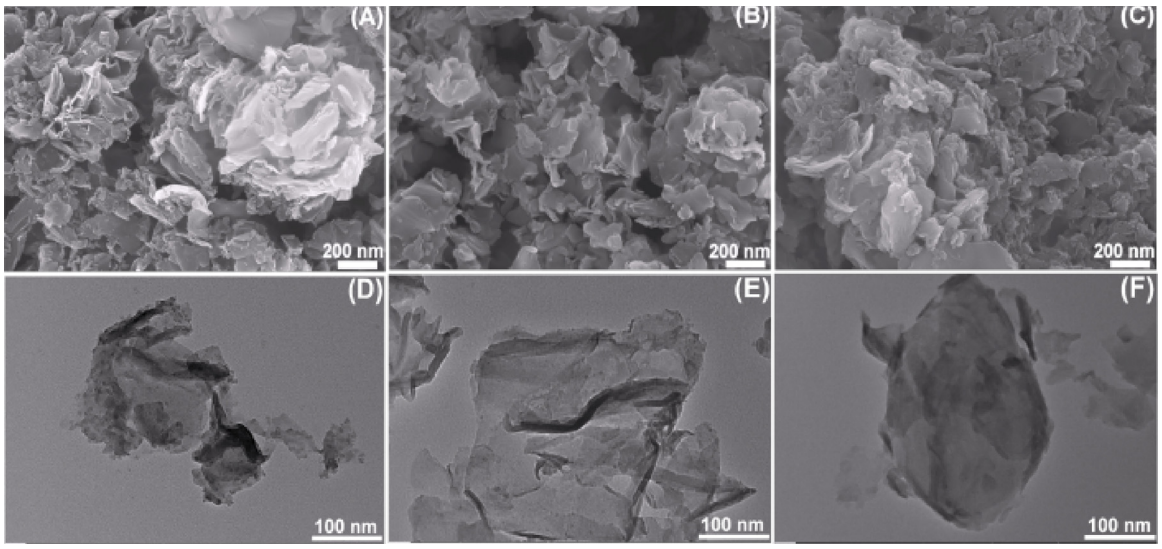

Figure 4. SEM and TEM images of Mg_3Al–EuW_{10} (A and D), Mg_3Al–TbW_{10} (B and E) and Mg_3Al–DyW_{10} (C and F).

reaction will be better promoted by the Ln^{3+} cations with larger radii. In conclusion, though the acidity and basicity of Mg_3Al–LnW_{10} (Ln = Eu, Tb and Dy) are similar, the different ionic radii of Ln^{3+} in Mg_3Al–LnW_{10} leads to different catalytic activities in cyanosilylation reaction.

Effect of solvents on cyanosilylation of acetophenone has been investigated catalyzed by Mg_3Al–EuW_{10} (Fig. S12). The results reveal that the yield under solvent-free conditions is higher than those in solvents. Therefore, to obtain high yields, cyanosilylation of various aldehydes and ketones will proceed under solvent-free conditions.

To obtain the kinetic parameters for cyanosilylation of acetophenone, experiments have been performed with the acetophenone:TMSCN:EuW_{10} = 401:602:1 at 25 °C under solvent-free conditions. Yield and $\ln(C_t/C_0)$ are plotted against reaction time in Fig. 6A, in which C_0 and C_t are initial acetophenone concentration and acetophenone concentration at time t, respectively. The linear fit of the data reveals that the catalytic reaction exhibits pseudo-first-order kinetics for the cyanosilylation reaction (R^2 = 0.9933). The rate constant k of cyanosilylation can be determined to be 0.0067 min^{-1} on the basis of Eqs. (1) and (2). Cyanosilylation of acetophenone could be completed with the yield of 95% in 6 h. Thus, the catalyst of Mg_3Al–EuW_{10} exhibits high catalytic efficiency for cyanosilylation, and the catalytic reaction strictly obey pseudo-first-order kinetics with >99.9% selectivity of corresponding cyanohydrins.

$$\frac{-dC_t}{dt} = k \quad (1)$$

$$C_0 - C_t = kt \quad (2)$$

Cyanosilylation of various aldehydes and ketones catalyzed by Mg_3Al–EuW_{10} has been carried out at 25 °C under solvent-free conditions. All the corresponding cyanohydrins can be afforded in good yields with >99.9% selectivity of corresponding cyanohydrins (Table 3, Entries 1–32). The results indicate that cyanosilylation of electron-donating substituted benzaldehydes such as methyl- and methoxy-substituted benzaldehydes (Entries 2–7) proceed easier than that of electron-withdrawing substituted benzaldehydes such as chloro-, bromo- and nitro-substituted benzaldehydes (Entries 8–16). The Hammett plot for the cyanosilylation of para-substituted benzaldehyde derivatives gave the negative ρ value of −0.7582 (Fig. 6B), suggesting the formation of positive transition state catalyzed by Mg_3Al–EuW_{10} is part of the rate-limiting step.

It is worth noting that the cyanosilylation of benzaldehyde proceeds efficiently in >99.9% yield with Mg_3Al–EuW_{10} (benzaldehyde:TMSCN:EuW_{10} = 23,990:35,985:1) at 25 °C

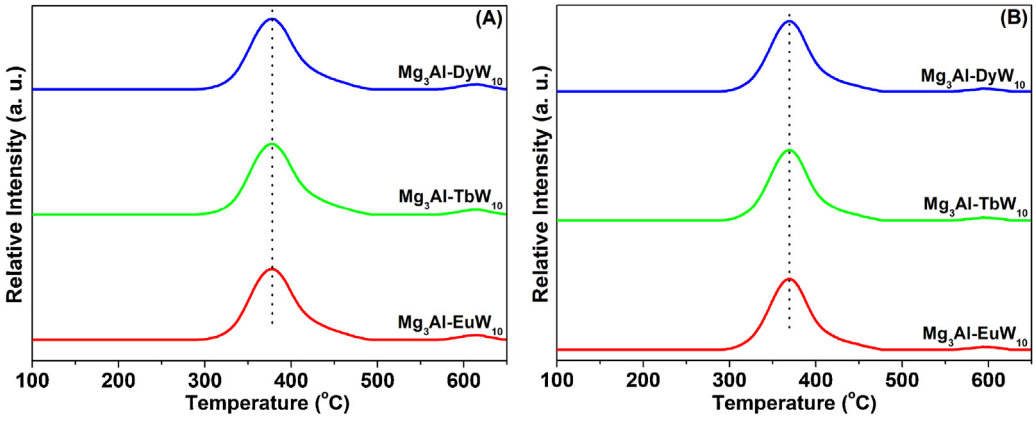

Figure 5. NH_3 (A) and CO_2 (B) TPD profiles of Mg_3Al–EuW_{10}, Mg_3Al–TbW_{10} and Mg_3Al–DyW_{10}.

Table 3
Cyanosilylation of various aldehydes and ketones with TMSCN catalyzed by Mg_3Al–EuW_{10} at 25 °C under solvent-free conditions.

Entry	Acceptor	Product	Time (h)	Yield (%)[a]
		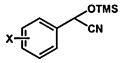		
1	X = H	X = H	2	98 (97)
2	X = 2-Me	X = 2-Me	1.5	>99.9 (98)
3	X = 3-Me	X = 3-Me	1.5	>99.9 (98)
4	X = 4-Me	X = 4-Me	1.5	>99.9 (99)
5	X = 2-MeO	X = 2-MeO	1.5	>99.9 (98)
6	X = 3-MeO	X = 3-MeO	1.5	>99.9 (99)
7	X = 4-MeO	X = 4-MeO	1.5	>99.9 (98)
8	X = 2-Cl	X = 2-Cl	3.5	>99.9 (99)
9	X = 3-Cl	X = 3-Cl	4	97 (95)
10	X = 4-Cl	X = 4-Cl	4	98 (96)
11	X = 2-Br	X = 2-Br	3.5	>99.9 (99)
12	X = 3-Br	X = 3-Br	4	97 (95)
13	X = 4-Br	X = 4-Br	4	>99.9 (99)
14	X = 2-NO_2	X = 2-NO_2	5	>99.9 (99)
15	X = 3-NO_2	X = 3-NO_2	5	>99.9 (98)
16	X = 4-NO_2	X = 4-NO_2	6	98 (96)
17		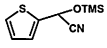	3	>99.9 (98)
18		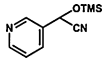	6	82 (78)
		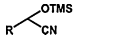		
19	R = n-C_5H_{11}	R = n-C_5H_{11}	2	97 (94)
20	R = n-C_6H_{13}	R = n-C_6H_{13}	2	96 (92)
21	R = n-C_7H_{15}	R = n-C_7H_{15}	2.5	97 (93)
22	R = n-C_8H_{17}	R = n-C_8H_{17}	2.5	98 (95)
23	R = n-C_9H_{19}	R = n-C_9H_{19}	2.5	99 (98)
24		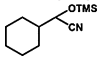	2	>99.9 (99)
25			6	95 (92)
				
26	R = n-C_5H_{11}	R = n-C_5H_{11}	3	>99.9 (97)
27	R = n-C_6H_{13}	R = n-C_6H_{13}	3	>99.9 (98)
28	R = n-C_7H_{15}	R = n-C_7H_{15}	3	99 (97)
29	R = n-C_8H_{17}	R = n-C_8H_{17}	3	99 (98)
30			1	>99.9 (98)
31			6	76 (71)
32			3	>99.9 (98)

Reaction conditions: substrate (1 mmol), Mg_3Al–EuW_{10} (0.25 mol% to substrate based on EuW_{10}), TMSCN (1.5 mmol), 25 °C. Yields were determined by GC analysis using reference standards. Assignments of corresponding cyanohydrins were analyzed by ^{1}H- and ^{13}C-NMR.
[a] The values in parentheses are the isolated yields.

under solvent-free conditions. The turnover number (TON) can reach as high as 23,990 (Table 4, Entry 1). Furthermore, the 10 g scale experiment of cyanosilylation of benzaldehyde can also proceed in >99.9 yield with the Mg_3Al–EuW_{10} (benzaldehyde:TMSCN:EuW_{10} = 119,950:179,925:1) at 25 °C under solvent-free conditions. The TON can reach as high as 119,950 (Entry 2), which is higher than that of LiCl in the 10 g scale experiment of cyanosilylation of benzaldehyde (TON = 100,000, Entry 5) at 25 °C in THF [27]. To the best of our knowledge, the TON for Mg_3Al–EuW_{10}-catalyzed cyanosilylation of benzaldehyde is the highest among previously reported values, which is higher than other catalysts including LiCl in THF (TON = 100,000, Entry 3) [27], $Sc(OTf)_3$ in [bmim][SbF_6] (TON =10,000, Entry 6) [28], $TBA_8H_2[(\gamma\text{-}SiYW_{10}O_{36})_2]\cdot 7H_2O$ (TBA–$Y_2(SiW_{10})_2$) in 1,2-dichloroethane (TON = 9400, Entry 7) [29], Au nanoparticles in chloroform (TON = 869, Entry 9) [30], Eu^{3+}-MCM-41 under solvent-free conditions (TON = 137, Entry 10) [25a], supported OH^- ionic liquid in dichloromethane (TON = 35.7, Entry 11) [31], supported Sc triflate in dichloromethane (TON = 20.4, Entry 12) [32], $Yb(OTf)_2$ in dichloromethane (TON = 17.2, Entry13) [33], $Cu(OTf)_2$ in dichloromethane (TON =16.2, Entry 15) [34], $P(MeNMCH_2CH_3)_3N$ in THF (TON = 9.2, Entry 16) [35], Bu_2SnCl_2 under solvent-free conditions (TON = 9, Entry 17) [36], and other catalysts (Entries 18–20 and 22–26) [37–39].

Furthermore, the cyanosilylation of hexanal proceeds efficiently in >99.9% yield with Mg_3Al–EuW_{10} (hexanal:TMSCN:EuW_{10} = 23,981:35,972:1) under solvent-free conditions at 25 °C. The TON can reach as high as 23,981 (Entry 3). The 10 g scale experiment of cyanosilylation of hexanal

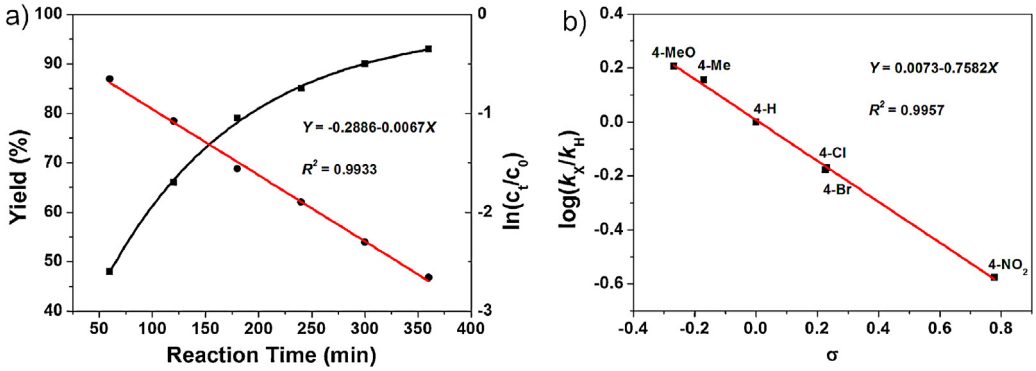

Figure 6. (A) Kinetic profiles of cyanosilylation of acetophenone catalyzed by Mg_3Al–EuW_{10} [square dot: yield of cyanohydrins; round dot: $\ln(C_t/C_0)$]; (B) Hammett plot for the cyanosilylation of benzaldehyde and *p*-substituted benzaldehyde derivatives. Reaction conditions: benzaldehyde or *p*-substituted benzaldehyde (1.0 mmol), Mg_3Al–EuW_{10} (0.25 mol% to substrate based on EuW_{10}), TMSCN (1.5 mmol), 25 °C.

can also proceed in >99.9 yield with the Mg_3Al–EuW_{10} (hexanal:TMSCN:EuW_{10} = 119,906:179,859:1) at 25 °C under solvent-free conditions. The TON can reach as high as 119,906 (Entry 4). To the best of our knowledge, the TON for Mg_3Al–EuW_{10}-catalyzed cyanosilylation of hexanal is the highest among previously reported values, and is higher than other catalysts such as $TBA_8H_2[(\gamma\text{-}SiYW_{10}O_{36})_2]\cdot 7H_2O$ (TBA–$Y_2(SiW_{10})_2$) in 1,2-dichloroethane (TON = 18,000, Entry 8) [29], $Yb(OTf)_2$ in dichloromethane (TON = 47.5, Entry 14) [33], and $Zr(KPO_4)_2$ in dichloromethane (Entry 21) [38].

From the above results, it can be seen clearly that to the best of our knowledge, Mg_3Al–EuW_{10}-catalyzed cyanosilylation of benzaldehyde and hexanal gives the highest TON of 119,950 and 119,906, respectively. Such cyanosilylation reaction can proceed efficiently at 25 °C and under solvent-free conditions. Moreover, the heterogeneous catalyst of Mg_3Al–EuW_{10} can be easily recovered and reused.

To confirm the catalysis is truly heterogeneous, cyanosilylation of acetophenone with TMSCN has been selected as an example by applying Mg_3Al–EuW_{10} as catalyst at 25 °C under solvent-free conditions. When the product yield reaches about 50%, Mg_3Al–EuW_{10} is removed from the reaction mixture by filtration, and the reaction is allowed to proceed with the filtrate under the same conditions. It can be found that no product can be obtained by adding more TMSCN. ICP-AES measurement reveals there is no Mg, Al, W and Eu content in the filtrate. These results rule out the contribution of Mg, Al, W and Eu species leached into the reaction solution for the observed catalytic results. Therefore, the catalytic reaction is truly heterogeneous.

Table 4
Comparison of yields and TONs for the cyanosilylation catalyzed by different catalysts.

Entry	Catalyst	Substrate	Solvent	*T* (°C)	*t* (h)	Yield (%)	TON[a]	Ref.
1	Mg_3Al–EuW_{10}	Benzaldehyde[b]	None	25	6	>99.9	23,990	This work
2	Mg_3Al–EuW_{10}	Benzaldehyde[c]	None	25	8	>99.9	119,950	This work
3	Mg_3Al–EuW_{10}	Hexanal[d]	None	25	6	>99.9	23,981	This work
4	Mg_3Al–EuW_{10}	Hexanal[e]	None	25	8	>99.9	119,906	This work
5	LiCl	Benzaldehyde[f]	THF	25	48	>99.9	100,000	[27]
6	$Sc(OTf)_3$	Benzaldehyde	[bmim][SbF_6]	25	0.5	>99.9	10,000	[28]
7	TBA–$Y_2(SiW_{10})_2$[g]	Benzaldehyde	1,2-Dichloroethane	25	0.25	94	9400	[29]
8	TBA–$Y_2(SiW_{10})_2$	Hexanal	1,2-Dichloroethane	25	0.03	90	18,000	[29]
9	Au nanoparticles	Benzaldehyde	Chloroform	25	4	93	869	[30]
10	Eu^{3+}-MCM-41	Benzaldehyde	None	25	1	90	137	[25a]
11	Supported OH^- ionic liquid	Benzaldehyde	Dichloromethane	32	0.5	>99.9	35.7	[31]
12	Supported Sc triflate	Benzaldehyde	Dichloromethane	25	3	95	20.4	[32]
13	$Yb(OTf)_2$	Benzaldehyde	Dichloromethane	25	15	86	17.2	[33]
14	$Yb(OTf)_2$	Hexanal	Dichloromethane	25	2	95	47.5	[33]
15	$Cu(OTf)_2$	Benzaldehyde	Dichloromethane	25	3	81	16.2	[34]
16	$P(MeNMCH_2CH_3)_3N$	Benzaldehyde	THF	0	1	92	9.2	[35]
17	Bu_2SnCl_2	Benzaldehyde	None	25	0.5	90	9	[36]
18	Sn–W mixed oxide	Benzaldehyde	1,2-Dichloroethane	23	0.5	99	–	[37]
19	Al^{3+}-MCM-41	Benzaldehyde	Dichloromethane	25	0.08	>99.9	–	[25b]
20	$Zr(KPO_4)_2$	Benzaldehyde	Dichloromethane	Reflux	0.3	98	–	[38]
21	$Zr(KPO_4)_2$	Hexanal	Dichloromethane	Reflux	0.2	83	–	[38]
22	Fe-Mont	Benzaldehyde	Dichloromethane	0	0.2	96	–	[39]
23	CaF_2	Benzaldehyde	Dichloromethane	0	0.5	99	–	[39]
24	HAp	Benzaldehyde	Dichloromethane	0	0.3	95	–	[39]
25	CaO	Benzaldehyde	Dichloromethane	0	0.2	96	–	[39]
26	MgO	Benzaldehyde	Dichloromethane	0	0.2	95	–	[39]

[a] TON (turnover number) = mole of corresponding product/mole of catalyst used.
[b] Benzaldehyde (5.3 g, 50 mmol), benzaldehyde:TMSCN:EuW_{10} = 23,990:35,985:1.
[c] Benzaldehyde (10.6 g, 100 mmol), benzaldehyde:TMSCN:EuW_{10} = 119,950:179,925:1.
[d] Hexanal (5.0 g, 50 mmol), benzaldehyde:TMSCN:EuW_{10} = 23,981:35,972:1.
[e] Hexanal (10.0 g, 100 mmol), benzaldehyde:TMSCN:EuW_{10} = 119,906:179,859:1.
[f] Benzaldehyde (10.6 g, 100 mmol), benzaldehyde:TMSCN:LiCl = 100,000:100,000:1.
[g] TBA–$Y_2(SiW_{10})_2$: $TBA_8H_2[(\gamma\text{-}SiYW_{10}O_{36})_2]\cdot 7H_2O$.

Successful recovery of the heterogeneous Mg_3Al–EuW_{10} can be achieved in the cyanosilylation of acetophenone through centrifugation after the reaction. The powder XRD, FT-IR, XPS, TPD (Fig. S14) and BET results (Table 1) reveal that the structure of the Mg_3Al–EuW_{10} remains unchanged. The yields of corresponding products remain unchanged and the yields for catalyst recovery of Mg_3Al–EuW_{10} are above 96% (Fig. S15). The ICP results (Table S10) also reveal that the composition of reused the Mg_3Al–EuW_{10} remains unchanged. All these results reveal that the structure and composition of Mg_3Al–EuW_{10} is not affected by the cyanosilylation and Mg_3Al–EuW_{10} is stable before and after cyanosilylation.

The mechanism of cyanosilylation by Mg_3Al–EuW_{10} can be proposed as following: the EuW_{10} in the gallery of LDHs can activate the carbonyl groups of substrates to form positive transition state, as suggested by the Hammett plot, which is followed by the nucleophilic addition to the activated substrates with TMSCN to form the corresponding cyanohydrins.

4. Conclusions

To summarize, the intercalation of the lanthanide-containing POMs into LDHs by the spontaneous flocculation method has led to the formation of a series of new Mg_3Al–EuW_{10}, Mg_3Al–TbW_{10} and Mg_3Al–DyW_{10}. The spontaneous flocculation method not only prevents Mg^{2+}/Al^{3+} cations leaching out of the LDHs during the intercalation reaction and successfully control the final Mg^{2+}/Al^{3+} ratio in the Mg_3Al–POMs, but also shows no co-formation of the impurity phase.

The application of Mg_3Al–EuW_{10} for cyanosilylation of various aldehydes and ketones under solvent-free conditions shows that the acid and base cooperative effect of Mg_3Al–EuW_{10} plays a significant role for the highly efficient catalytic activity in cyanosilylation of various aldehydes and ketones. As far as we know, Mg_3Al–EuW_{10}-catalyzed cyanosilylation of benzaldehyde and hexanal give the highest TON of 119,950 and 119,906, respectively; cyanosilylation catalyzed by Mg_3Al–EuW_{10} can proceed efficiently at 25 °C and under solvent-free conditions without the environmental-unfriendly solvents of THF, dichloromethane, 1,2-dichloroethane and chloroform; Mg_3Al–EuW_{10} can be easily recovered and reused for at least 10 times without obvious decrease of catalytic activities. The structure and the composition of the Mg_3Al–POMs catalysts remain untouched. The easy preparation, reusability, and efficiency of the heterogeneous catalysts of Mg_3Al–EuW_{10} provide great potential for industrial application.

Acknowledgments

This research was supported by National Basic Research Program of China (973 program, 2014CB932104), National Science Foundation of China (21222104), Key Laboratory of Polyoxometalate Science of Ministry of Education (Northeast Normal University), Fundamental Research Funds for the Central Universities (RC1302) and the Program for Changjiang Scholars and Innovative Research Team in University.

Appendix A. Supplementary data

Supplementary data associated with this article can be found, in the online version, at http://dx.doi.org/10.1016/j.apcata.2014.09.005.

References

[1] (a) C.L. Hill, Chem. Rev. 98 (1998) 1–390, Special issue on polyoxometalates, Guest Editor;
(b) L. Cronin, A. Müller, Chem. Soc. Rev. 41 (2012) 7333–7334;
(c) A. Proust, B. Matt, R. Villanneau, G. Guillemot, P. Gouzerh, G. Izzet, Chem. Soc. Rev. 41 (2012) 7605–7622;
(d) M. Nymanz, P.C. Burns, Chem. Soc. Rev. 41 (2012) 7354–7367;
(e) Y.F. Song, R. Tsunashima, Chem. Soc. Rev. 41 (2012) 7384–7402.
[2] (a) H. Lv, Y.V. Geletii, C. Zhao, J.W. Vickers, G. Zhu, Z. Luo, J. Song, T. Lian, D.G. Musaev, C.L. Hill, Chem. Soc. Rev. 41 (2012) 7572–7589;
(b) P. Yin, D. Li, T. Liu, Chem. Soc. Rev. 41 (2012) 7368–7383;
(c) I.V. Kozhevnikov, Catalysis by Polyoxometalates, Wiley, Chichester, 2002;
(d) D.L. Long, R. Tsunashima, L. Cronin, Angew. Chem. Int. Ed. 49 (2010) 1736–1758.
[3] V. Rives, D. Carriazo, C. Martin, in: A. Gill, S.A. Korili, R. Trujillano, M.A. Vicentè (Eds.), Springer, New York, 2010, 319–422.
[4] (a) S.K. Yun, T.J. Pinnavaia, Inorg. Chem. 35 (1996) 6853–6860;
(b) B. Sels, D. De Vos, M. Buntinx, F. Pierard, A. Kirsch-De Mesmaeker, P.A. Jacobs, Nature 400 (1999) 855–857;
(c) P. Liu, C. Wang, C. Li, J. Catal. 262 (2009) 159–168;
(d) S. Zhao, J. Xu, M. Wei, Y.F. Song, Green Chem. 13 (2011) 384–389.
[5] (a) F. Cavani, F. Trifiró, A. Vaccari, Catal. Today 11 (1991) 173–301;
(b) V. Rives, M.A. Ulibarr, Coord. Chem. Rev. 181 (1999) 61–120;
(c) Q. Wang, D. O'Hare, Chem. Rev. 112 (2012) 4124–4155;
(d) M. Osada, T. Sasaki, Adv. Mater. 24 (2012) 210–288;
(e) C. Yu, J. He, Chem. Commun. 48 (2012) 4933–4940.
[6] B.F. Sels, D.E. De Vos, P.A. Jacobs, Catal. Rev. 43 (2001) 443–488.
[7] S. Omwoma, W. Chen, R. Tsunashima, Y.F. Song, Coord. Chem. Rev. 258–259 (2014) 58–71.
[8] S. Cho, J. Kwag, S. Jeong, Y. Baek, S. Kim, Chem. Mater. 25 (2013) 1071–1077.
[9] J.L. Gunjakar, T.W. Kim, H.N. Kim, I.Y. Kim, S. Hwang, J. Am. Soc. Chem. 133 (2011) 14998–15007.
[10] (a) L. Li, R. Ma, Y. Ebina, K. Fukuda, K. Takada, T. Sasaki, J. Am. Soc. Chem. 129 (2007) 8000–8007;
(b) S. Werner, V.W. Lau, S. Hug, V. Duppel, H. Clausen-Schaumann, B.V. Lotsch, Langmuir 29 (2013) 9199–9207;
(c) S. Cho, S.C. Hong, S. Kim, J. Mater. Chem. C 2 (2014) 450–457.
[11] R.D. Peacock, T.J.R. Weakley, J. Chem. Soc. A (1971) 1836–1839.
[12] N. Iyi, Y. Ebina, T. Sasaki, J. Mater. Chem. 21 (2011) 8085–8095.
[13] Z. Liu, R. Ma, M. Osada, N. Iyi, Y. Ebina, K. Takada, T. Sasaki, J. Am. Chem. Soc. 128 (2006) 4872–4880.
[14] N. Iyi, H. Yamada, T. Sasaki, Appl. Clay Sci. 54 (2011) 132–137.
[15] Z. Han, Y. Guo, R. Tsunashima, Y.F. Song, Eur. J. Inorg. Chem. 9 (2013) 1475–1480.
[16] F.L. Sousa, M. Pillinger, R.A. Sá Ferreira, C.M. Granadeiro, A.M.V. Cavaleiro, J. Rocha, L.D. Carlos, T. Trindade, H.I.S. Nogueira, Eur. J. Inorg. Chem. (2006) 726–734.
[17] Y. Zhao, F. Li, R. Zhang, D.G. Evans, X. Duan, Chem. Mater. 14 (2002) 4286–4291.
[18] K. Nakamoto, Infrared and Raman Spectra of Inorganic and Coordination Compounds, 4th ed., John Wiley and Sons, New York, 1986, pp. 137–141.
[19] J.T. Kloprogge, R.L. Frost, J. Solid State Chem. 146 (1999) 506–515.
[20] Z.P. Xu, H.C. Zeng, Chem. Mater. 13 (2001) 4555–4563.
[21] J. Rocha, M. del Arco, V. Rives, M.A. Ulibarri, J. Mater. Chem. 9 (1999) 2499–2503.
[22] (a) M.A. Aramendía, V. Borau, C. Jiménez, J.M. Marinas, J.R. Ruiz, F.J. Urbano, Appl. Catal. A: Gen. 255 (2003) 301–308;
(b) P.J. Siders, F. Blanc, Z. Gan, C.P. Grey, Chem. Mater. 24 (2012) 2449–2461.
[23] K.S.W. Sing, D.H. Everett, R.A.W. Haul, L. Moscou, R.A. Pierotti, J. Rouquerol, T. Siemieniewska, Pure Appl. Chem. 57 (1985) 603–620.
[24] (a) J.M. Brunel, I.P. Holmes, Angew. Chem. Int. Ed. 43 (2004) 2752–2778;
(b) P. Sreekanth, S.W. Kim, T. Hyeon, B.M. Kim, Adv. Synth. Catal. 345 (2003) 936–938;
(c) R.J.H. Gregory, Chem. Rev. 99 (1999) 3649–3682.
[25] (a) A. Procopio, G. Das, M. Nardi, M. Oliverio, L. Pasqua, ChemSusChem 1 (2008) 916–919;
(b) K. Iwanami, J.C. Choi, B. Lu, T. Sakakura, H. Yasuda, Chem. Commun. (2008) 1002–1004.
[26] (a) J.J. Song, F. Gallou, J.T. Reeves, Z. Tan, N.K. Yee, C.H. Senanayake, J. Org. Chem. 71 (2006) 1273–1276;
(b) S.E. Denmark, W.J. Chung, J. Org. Chem. 71 (2006) 4002–4005.
[27] N. Kurono, M. Yamaguchi, K. Suzuki, T. Ohkuma, J. Org. Chem. 70 (2005) 6530–6532.
[28] B.Y. Park, K.Y. Ryu, J.H. Park, S.G. Lee, Green Chem. 11 (2009) 946–948.
[29] Y. Kikukawa, K. Suzuki, M. Sugawa, T. Hirano, K. Kamata, K. Yamaguchi, N. Mizuno, Angew. Chem. Int. Ed. 51 (2012) 3686–3690.
[30] W.K. Cho, J.K. Lee, S.M. Kang, Y.S. Chi, H.S. Lee, I.S. Choi, Chem. Eur. J. 13 (2007) 6351–6358.
[31] K. Yamaguchi, T. Imago, Y. Ogasawara, J. Kasai, M. Kotani, N. Mizuno, Adv. Synth. Catal. 348 (2006) 1516–1520.
[32] B. Karimi, L. Ma'Mani, Org. Lett. 6 (2004) 4813–4815.
[33] Y. Yang, D. Wang, Synlett (1997) 1379–1380.
[34] P. Saravanan, R.V. Anand, V.K. Singh, Tetrahedron Lett. 39 (1998) 3823–3824.
[35] Z. Wang, B. Fetterly, J.G. Verkade, J. Organomet. Chem. 646 (2002) 161–166.
[36] J.K. Whitesell, R. Apodaca, Tetrahedron Lett. 37 (1996) 2525–2528.
[37] Y. Ogasawara, S. Uchida, K. Yamaguchi, N. Mizuno, Chem. Eur. J. 15 (2009) 4343–4349.
[38] M. Curini, F. Epifano, M.C. Marcotullio, O. Rosati, M. Rossi, Synlett (1999) 315–316.
[39] K. Higuchi, M. Onaka, Y. Izumi, Bull. Chem. Soc. Jpn. 66 (1993) 2016–2032.